ADVANCED MATERIALS

Supporting Information

for *Adv. Mater.*, DOI: 10.1002/adma.202000716

Turning Trash into Treasure: Additive Free MXene Sediment Inks for Screen-Printed Micro-Supercapacitors

Sina Abdolhosseinzadeh, René Schneider, Anand Verma, Jakob Heier, Frank Nüesch, and Chuanfang (John) Zhang**

Supporting Information

Turning Trash into Treasure: Additive Free MXene Sediment Inks for Screen-Printed Micro-Supercapacitors

Sina Abdolhosseinzadeh, René Schneider, Anand Verma, Jakob Heier, Frank Nüesch, Chuanfang (John) Zhang**

Methods

Etching of the MAX. The etching of the MAX phase was performed using a minimally intensive layer delamination or "MILD" synthesis route. Typically, 0.5 g of lithium fluoride (LiF, Sigma Aldrich, USA) was slowly added to 10 mL, 9 M hydrochloric acid (HCl, 37 wt%, Sigma Aldrich, USA) under vigorous stirring at room temperature. After the complete dissolution of LiF in HCl, 0.5 g of Ti_3AlC_2 MAX phase (average particle size ~38 µm, Y-Carbon, Ukraine) was slowly added to the above mixture under vigorous stirring, then reacted for 24 h at room temperature at a stirring speed of 300 rpm. Once the reaction ended, the suspension was transferred to centrifuge tubes and centrifuged at 1500 rcf for 3 min. After the centrifugation, the supernatant was decanted, and 40 mL of fresh DI water was added to the suspension followed by vigorous shaking for 1 min, then subjected to another round of centrifugation at 3500 rcf for 3 min. This washing process was repeated 5 times until the pH of the supernatant became ~6. The sediments are etched MAX.

Formulation of MXene sediment inks. To prepare the sediment inks, delamination of the etched MAX is necessary. In the etched MAX, the multi-layered MXene can be further exfoliated by a manual shaking method as reported in REF[39]. After vigorously shaking the etched MAX suspension, the multi-layered MXene can be delaminated into few-layered or

mostly single-layered MXene nanosheets. Further centrifuging separates the delaminated nanosheets from the multi-layered MXene and un-etched MAX. Therefore, after decanting the supernatant, the sediments are usually trashed away. However, these sediments could be further formulated to become a valuable printable ink to print various patterns or devices. Three main parameters were considered upon sediment ink formulation: rheological properties (suitable for screen printing), high solid content, and adhesion/mechanical stability of the printed traces. Since increasing the ratio of mono- or few-layered MXene to unetched MAX and m-MXene limits the highest attainable solid content, the minimum amount of the well delaminated MXene which was necessary for a good mechanical stability of the films was kept. The rheological properties were fine-tuned by addition of water. As such, after vigorously shaking the as-etched MAX suspension for 40 min with a vortex mixer (VORTEXER-Heathrow) at 3000 rpm, centrifugation was performed at 1500 rcf for 30 min. After collecting the supernatant-delaminated MXene nanosheets, we left 2 wt.% of delaminated MXene nanosheets in the centrifuge tube and added a required amount of DI-water with solid content set to 22 wt.%, followed by a three-roll mill processing to form a homogeneous sediment ink.

Screen designing. Two screens were used, equipped with either a standard PET mesh (150/31; 22.5°) and coated by hand with an all-round photoemulsion (FLX Screen; Siebdruckversand, Germany) or with a stainless steel mesh (159/18; 45°) coated with Polycol Micro (EOM 15 ± 2µm from Kiwo, Germany). Printed structures are simple lines for conductivity and bending experiments with line lengths of 10 mm and various width from 200 - 1000 µm. Furthermore, interdigitated structures with various line widths and gaps ranging from 100 - 500 µm were designed to print micro-supercapacitors (MSCs). Interdigitated structures with 50 µm gap, which is close to the resolution of the screen printing method (25-30 µm), can be printed but the number of overprint passes can hardly exceed 2 (since by

spreading of the ink, fingers will merge). Hence, larger gaps (e.g. 100-200 μm) are preferred for overlayer printing. Existence of large particles in the sediment ink is another limiting factor for increasing of the print resolution.

Screen printing of various patterns. Screen printing was performed on the multifunctional sheet-to-product printer C600 manufactured by nsm Norbert Schläfli AG, Switzerland. The printer hosts a gravure-, flexo- and screen printing unit, as well as a hot air Comb Nozzle® dryer from CN drying technology, Germany. A high repeat accuracy of the nsm C600 was demonstrated in previous work.[55] Devices were printed on office paper (Canon Pixma HR-101N) and glossy photo paper (Epson C13S041706) with lift-off set to 0.800 mm, printing speed was 50 mm/s and the squeegee (RKS Carbon S 65) angle was 71.5° ± 0.5°. Squeegee height was set 30 μm below the actual substrate thickness to achieve an appropriate printing pressure. Multilayer printing was performed with drying at 80°C between each printed path.

Materials characterization.

Delaminated MXene nanosheets were imaged by TEM and SEM images. The width of printed lines was measured along the axial direction of the SEM images. The spatial uniformity was obtained from the width variation statistics. Height profiles of the as-printed lines were acquired with a non-destructive, confocal 3D Optical Surface Metrology System (DCM8, Leica Microsystems AG, Switzerland). Measurements were taken with Leica EPI 20x objective in confocal mode. Data were analyzed with the Leica Map 7.2 software. The average layer thickness was determined by subtracting the height of a printed area of the height of a substrate area. Atomic force microscopy (AFM) images were taken with an ICON3 from Bruker, Karlsruhe, Germany in the peak force tapping mode. The rheological behaviour of $Ti_3C_2T_x$ (Tx represents surface terminal groups such as -OH, -F, -Oetc.) sediment inks was studied on an Anton Paar MCR 301 rheometer using a PP25, parallel plate

geometry (diameter of 25 mm, gap of 1 mm). All the loaded samples were allowed to equilibrate at room temperature for 1 minute. Oscillatory strain sweeps were performed first at a frequency of 0.5 Hz, from 0.01-100% strain, with consecutive measurements performed to ensure reproducibility. Apparent viscosities of the inks were measured *via* steady-state continuous shear experiments with a sweep of shear rate (0.1-100 s^{-1}).

Raman spectra of vacuum-filtrated films made of delaminated nanosheets, as well as the screen-printed lines one paper and on glass, were acquired on a Renishaw Raman microscope. The excitation wavelength was 633 nm and the amplitude sweep frequency was 10 Hz. The sheet resistance of the as-printed lines was measured using a four-point probe method (Jandel RM3-AR, UK). The sheet resistance of the lines with different passes was converted to the electrical conductivity based on the line thickness which was measured through the optical microscopy.

To measure the mechanical flexibility of the as-printed lines, the screen-printed lines (with or without delaminated MXene nanosheets) were cut into strips with two ends fixed to the substrate using the tap. Two short Ag paints were coated on the two ends, which was connected to a multimeter through two pieces of Cu wire. To ensure good contact, two pieces of tap were tightly covered on the Ag paints and Ag-Cu connecting point. The resistances of the strips upon bending for different degrees and cycles were recorded. One cycle is defined as bending the flat strip to 180° and then released to the flat state. For the cycling tests, the strips were bent for 15000 cycles with the resistance recorded through the multimeter.

Solid-state, on-chip MSC fabrication. The as-printed $Ti_3C_2T_x$ MXene interdigitated patterns were further used to fabricate MSC devices. Due to its excellent metallic conductivity, $Ti_3C_2T_x$ MXene-based MSC requires no additional current collector or conductive agents or polymeric binders, and thus acts as both the active material and current collector for MSCs. To facilitate the measurements, we glued two Ag wires at the end of the MSC by Ag paint and

allowed it to dry for 10 min. Then a piece of tape was tightly placed on the Ag paint to avoid the latter from direct contact with the electrolyte. After that, the as-printed MSCs were coated with a layer of gel-like polymer electrolyte made of 3M sulfuric acid (H_2SO_4)-poly(vinyl alcohol, PVA) gel electrolyte. For the preparation of the gel electrolyte we followed the procedure reported in ref [37]. After drying at ambient atmosphere, solid-state, coplanar on-chip MSCs were formed, which were stored under vacuum for further measurements.

Electrochemical characterization. The charge storage performance of the as-fabricated MSCs was evaluated through CV and GCD on a VMP3 potentiostat (BioLogic, France). The devices were tested at different CV scan rates (from 5 to 1000 mV/s) and GCD current densities (from 0.02 to 2.4 mA/cm^2) in a voltage window of 0.6 V. The cycling performance of the devices was evaluated at 1.2 mA using the MSC with finger gap=400 μm and <N>=5. Electrochemical impedance spectroscopy was performed at open-circuit voltage from 100 mHz to 100 kHz. The areal capacitance per electrode was calculated from the stabilized (fifth) CV curve according to the following equation:

$$C/A = \frac{4}{A_t \Delta V \nu} \int_0^{0.6} j dV \quad (1)$$

Where, *C/A* is the measured areal capacitance (mF/cm^2), j is the current (mA), ΔV is the voltage window (0.5 V), A_t (cm^2) is the geometric area of the MSC, υ is the scan rate (mV/s).

In the devices that showcased symmetric, linear GCD curves, the areal capacitance was also obtained from the stabilized (fifth) GCD curves according to the following equation:

$$C/A = \frac{4 j \Delta t}{A_t \Delta V} \quad (2)$$

Where ΔV is the effective voltage window after the IR drop, Δt is the discharge time.

For the Ragone plot, the device areal energy density and power density were calculated based on the following equations:

$$\frac{C_D}{A} = \frac{\int_0^{0.6} jdV}{A_t \Delta V \upsilon} \quad (4)$$

$$\frac{E_D}{A} = \frac{C_D \times V^2}{A \times 2 \times 3.6} \quad (5)$$

$$\frac{P_D}{A} = \frac{E_D \times \nu \times 3600}{A \times \Delta V} \quad (6)$$

Where C_D/A (mF/cm^2) is the areal capacitance of the device, E_D/A is the device areal energy density (μWh/cm^2), P_D/A is the device areal power density (μW/cm^2), j is the current (mA), ΔV is the voltage window (0.5 V), A_t (cm^2) is the geometric area of the MSC, υ is the scan rate (mV/s).

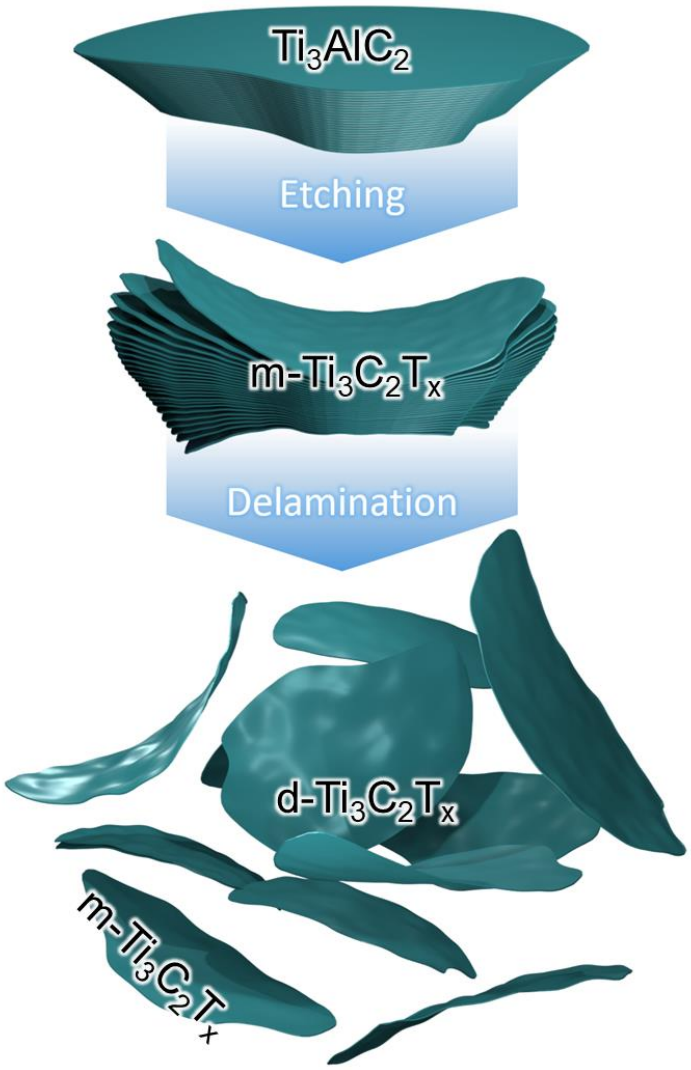

Supplementary Scheme 1. Illustration on MXene etching and delamination. Etching was performed in LiF-HCl mixture while delamination was performed using a manual shaking method.

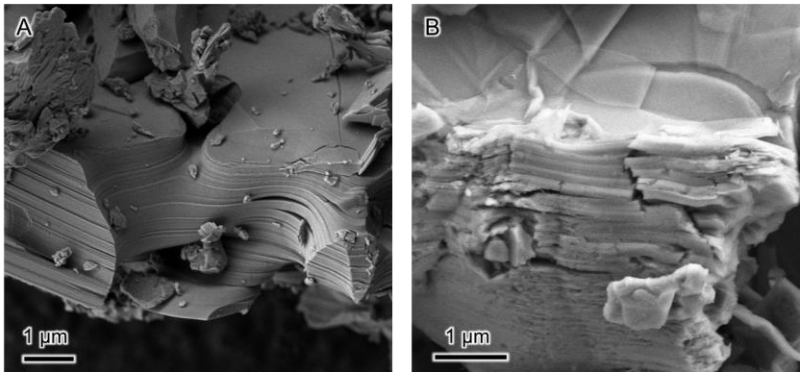

Supplementary Figure 1. Morphological characterization of MAX and MXene. SEM images of A, Ti_3AlC_2 MAX phase and B, as-obtained m-$Ti_3C_2T_x$ after washing the sediments. The multi-layered MXene shows a certain degree of delamination, which is attributed to the vigorous shaking during washing that facilitates the solvent exchange with pre-intercalated Li^+.

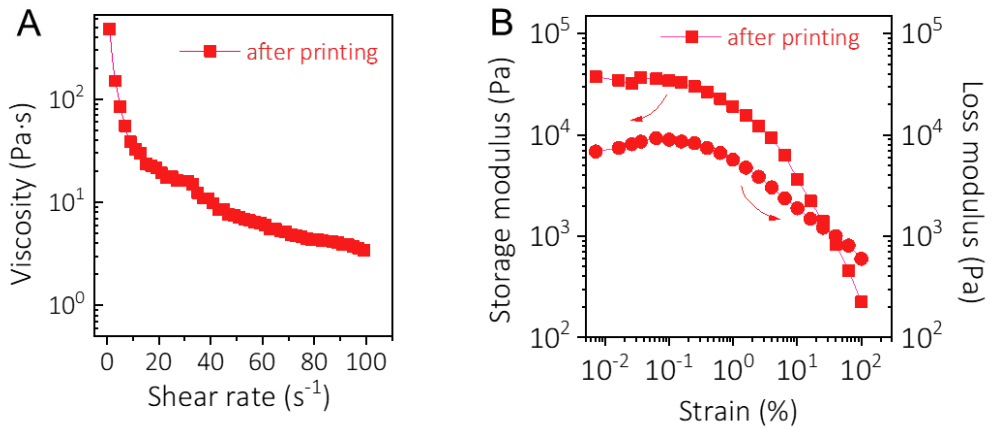

Supplementary Figure 2. A, Viscosity plotted as a function of shear rates of MXene inks after printing. B, Storage modulus and loss modulus plotted as a function of strain of MXene inks after printing.

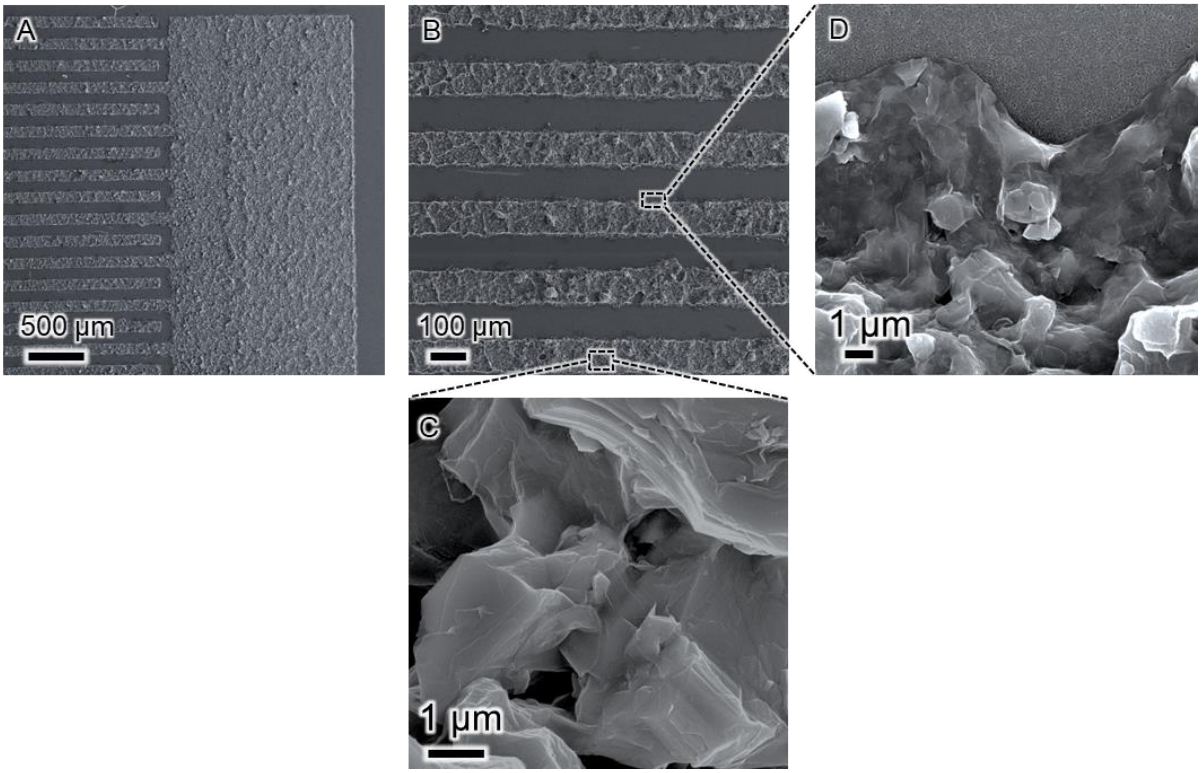

Supplementary Figure 3. Morphology characterizations of screen-printed $Ti_3C_2T_x$ MXene patterns. SEM image of the as-printed MXene-based interdigitated pattern at lower (A) and higher magnification (B), respectively. C, SEM image of the encircled area in B, showing the exist of multi-layered MXene, MAX phase and delaminated MXene nanosheets as a conductive binder. D, The zoom-in SEM image on the edge of as-printed line, showing the presence of delaminated nanosheets which tightly wrap the multi-layered particles.

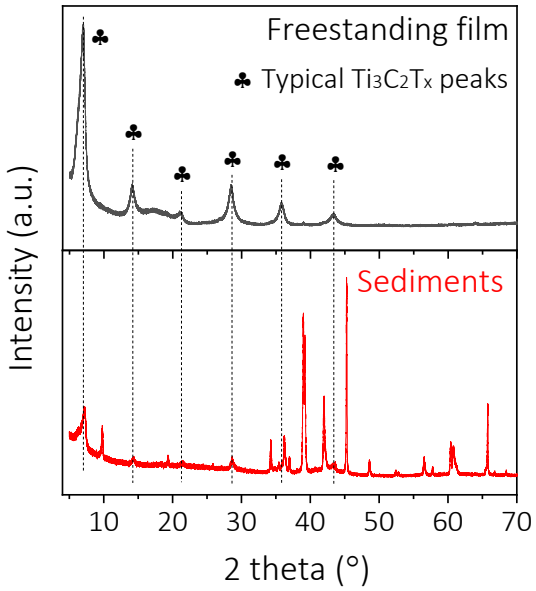

Supplementary Figure 4. Component study in the sediments. XRD patterns of MXene sediments and freestanding MXene film. It can be observed that typical $Ti_3C_2T_x$ peaks can be indexed in the sediments, indicating the presence of delaminated $Ti_3C_2T_x$ nanosheets. Moreover, peaks from the multi-layered $Ti_3C_2T_x$ and MAX can also be located, suggesting the hierarchical structure in the sediments.

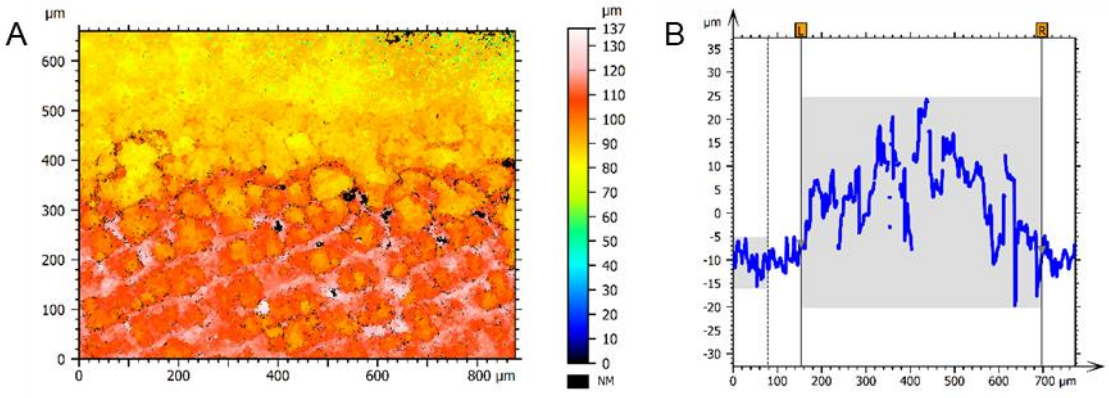

Supplementary Figure 5. A, Height analysis of the as-printed lines with <*N*>=4. The optical microscopy mapping of screen-printed MXene sediments. The surface is reasonably rough due to the multi-layered particles decorate everywhere. However, the conductive binder from

the delaminated $Ti_3C_2T_x$ nanosheets smoothen the surface to some extent, rendering the possibility of estimation of the height of the as-printed lines. B. Cross section and corresponding height profile of a printed 500 µm finger electrode.

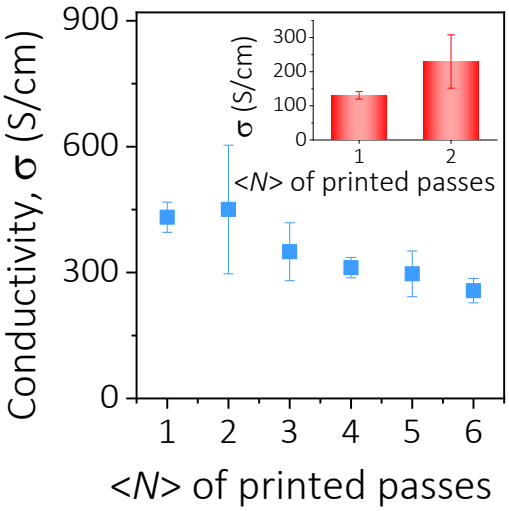

Supplementary Figure 6. Conductivity measurements of screen-printed lines with different number of passes. Inset is the conductivity of as-printed lines with different number of printed passes based on super-trash MXene sediment (without d-MXene nanosheets).

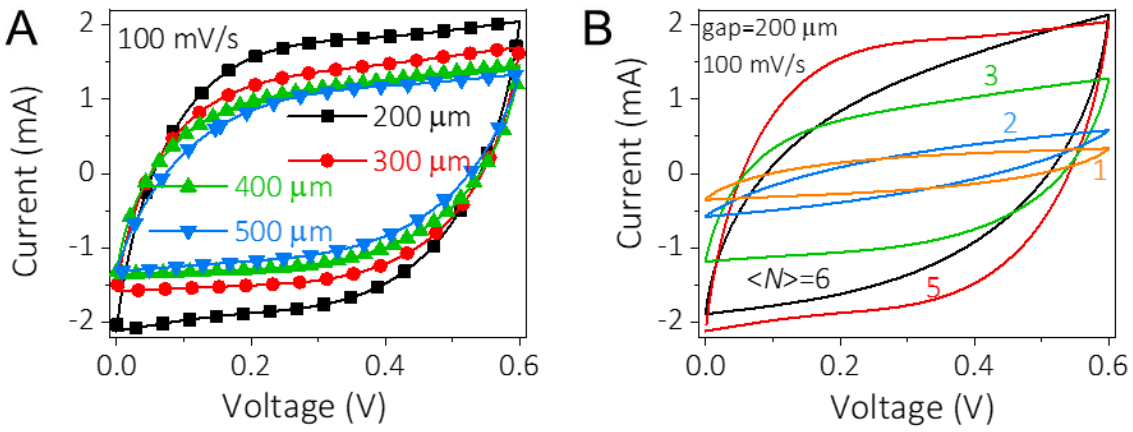

Supplementary Figure 7. Electrochemical response of screen-printed MSCs with different finger gaps (A) and number of printing passes (B), respectively.

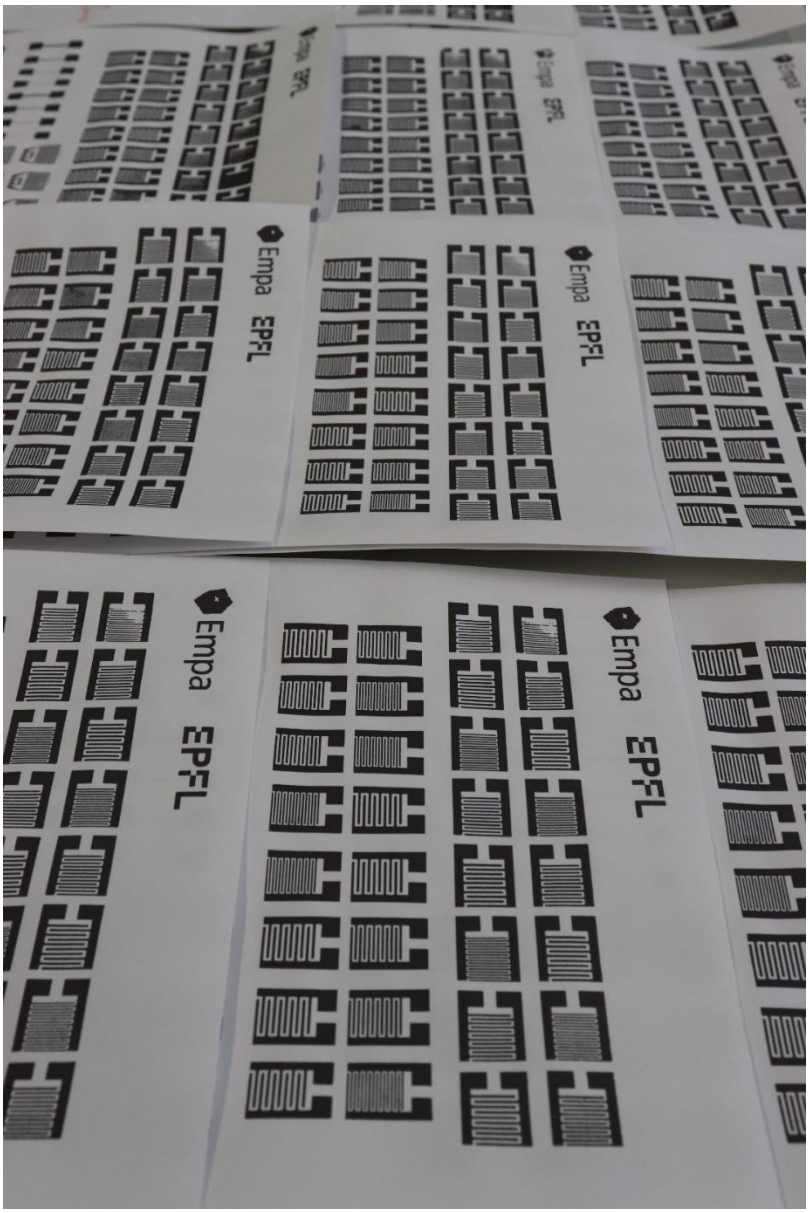

Supplementary Figure 8. Scale-up production of screen-printed MSCs based on MXene sediment inks. By adjusting the finger length/width, gaps and pass number, personalized MSCs with different line gaps/length/width/thickness can be easily screen-printed. Moreover, by designing the screen, and covering the inks above all the patterns, plenty of MSCs can be rapidly produced.

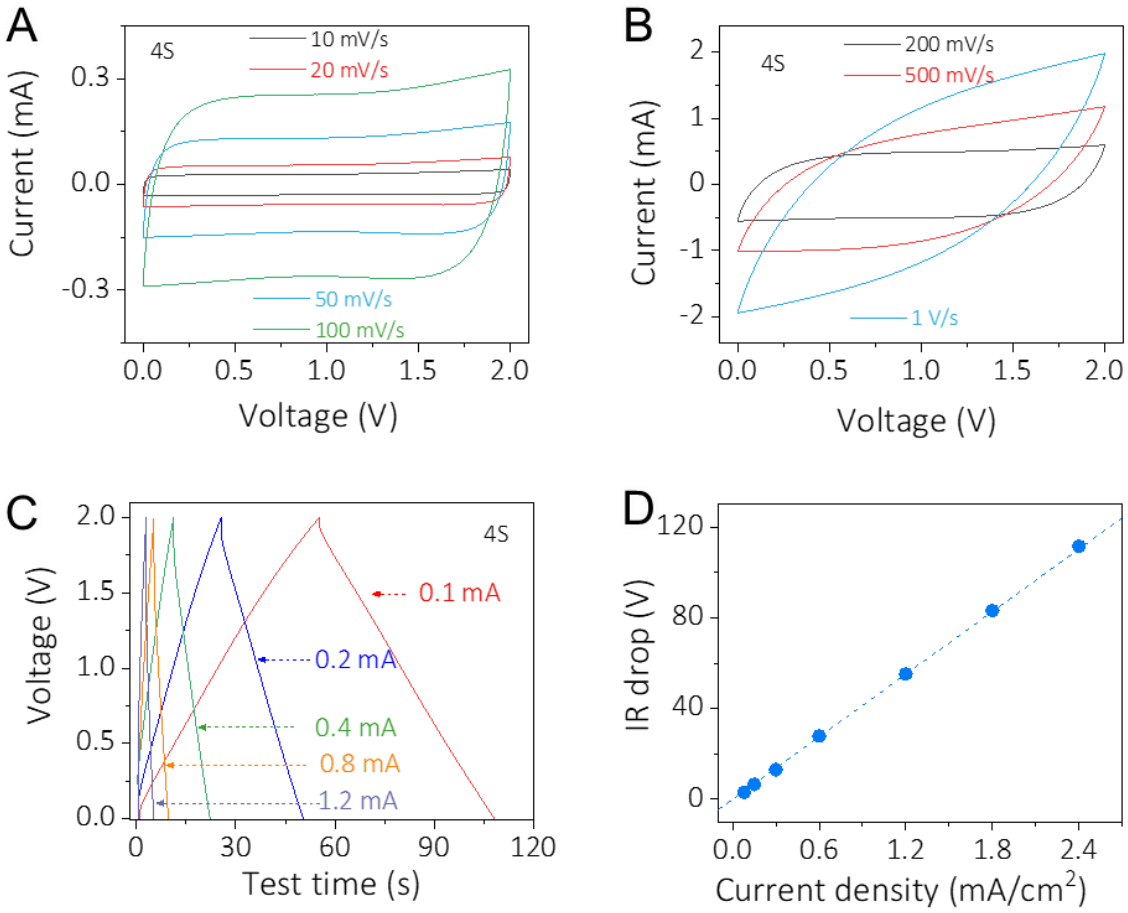

Supplementary Figure 9. Electrochemical characterization of MXene tandem device. CVs of 4 as-printed devices connected in series under 10-100 mV/s (A) and 200-1000 mV/s (B). (C), GCD curves of 4S tandem device, demonstrating a stable voltage window of 2 V. (D), IR drop of the tandem device at different current densities.

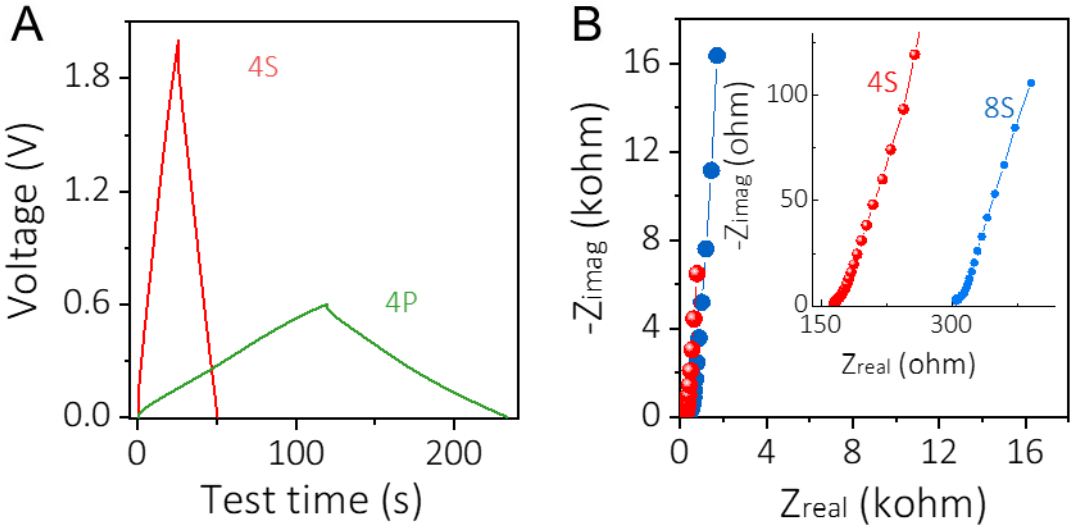

Supplementary Figure 10. Electrochemical characterizations of tandem devices. (A), GCD profiles of 4S and 4P (4 MSCs connected in parallel) tandem devices. (B), EIS Nyquist plot of 4S and 8S tandem devices, showing a negligible semicircle (reflective of charge transfer resistance) and a nearly perpendicular line in the low-frequency region (100 mHz). This suggests good capacitive or pseudocapacitive behaviors. Inset shows the plots in the low frequency region, showing a much smaller contact resistance (the X-axis intercept) in the 4S compared to that of 8S.

Supplementary Table 1. Areal capacitance comparison of various MSCs (Fig. 4G)

Material	**MSC fabrication method**	**Areal capacitance per electrode (C/A, mF/cm^2)**	**Reference**
Electrochemical exfoliated graphene	Inkjet printing	0.7	[3]
Exfoliated graphene	Spray coating	0.8	[4]
Graphene	Inkjet printing	0.82	[5]
Graphene/MXene (G-MX)	Spray coating	3.2	[6]
Graphene/PEDOT (G-PEDOT)	Spray coating	5.4	[4]
Graphene	Layer-by-layer printing	19.8	[7]
$Ti_3C_2T_x$ MXene	Laser scribing	24.8	[8]
$Ti_3C_2T_x$ MXene	Laser cutting	27	[9]
MnO_2/graphene	Spray coating	35	[10]
$Ti_3C_2T_x$ MXene	Extrusion printing	43	[11]
$Ti_3C_2T_x$ MXene	Stamping	57	[2]
PANi/graphene	filtration	119	[12]
MXene sediments	Screen printing	158	<N>=5, this work

Supplementary Table 2. Energy & power density comparison of various MSCs (Fig. 4H)

Sample	Power density (μW/cm^2)	Energy density (μWh/cm^2)	reference
Reduced graphene oxide (rGO)	9	0.014	[13]
PEDOT-Ag	138 575 1480 2290 2880	0.041 0.040 0.034 0.022 0.019	[8]
Inkjet-printed graphene (Inkjet, Gr.)	0.025 0.045 0.1 0.175 0.3	1.39E-03 1.25E-03 1.11E-03 9.72E-04 8.33E-04	[14]
Spray-coated graphene/PEDOT (PEDOT-Gr.)	0.8 1.6 3 5.6 12 20.8 40	0.089 0.071 0.067 0.062 0.053 0.046 0.044	[6]
Spray-coated graphene (Sprayed Gr.)	0.2 0.41 0.79 1.35	0.028 0.023 0.022 0.019	[6]

	2.81 4 5	0.016 0.011 0.0069	
Graphene quantum dots/MnO_2 (MnO_2-GQD)	7.5	0.15	[15]
Extrusion-printed all-MXene MSC (Extrusion, MX)	11.4 22.5 44.1 75.1 115.4 157.7	0.32 0.31 0.30 0.21 0.16 0.11	[11]
Stamped MXene MSC (Stamped, MX)	6.17 14.06 30.31 64.78 135.36 326.44	0.76 0.74 0.73 0.71 0.68 0.63	[2]
Screen-printed MXene sediment inks	18.46 37.11 75.57 156.98 334.99 544.12 778.33	1.64 1.62 1.57 1.51 1.42 1.36 1.32	This work

References

1. Zhang, C. J. *et al.* Transparent, Flexible, and Conductive 2D Titanium Carbide (MXene) Films with High Volumetric Capacitance. *Adv. Mater.* **29**, 1702678 (2017).
2. Zhang, C. J. *et al.* Stamping of Flexible, Coplanar Micro-Supercapacitors Using MXene Inks. *Adv. Funct. Mater.* **28**, 1705506 (2018).
3. Li, J. *et al.* Scalable Fabrication and Integration of Graphene Microsupercapacitors through Full Inkjet Printing. *ACS Nano* **11**, 8249–8256 (2017).
4. Liu, Z. *et al.* Ultraflexible In-Plane Micro-Supercapacitors by Direct Printing of Solution-Processable Electrochemically Exfoliated Graphene. *Adv. Mater.* **28**, 2217–2222 (2016).
5. Li, J. *et al.* Efficient Inkjet Printing of Graphene. *Adv. Mater.* **25**, 3985–3992 (2013).
6. Li, H. *et al.* Flexible All-Solid-State Supercapacitors with High Volumetric Capacitances Boosted by Solution Processable MXene and Electrochemically Exfoliated Graphene. *Adv. Energy Mater.* **7**, 1601847 (2017).
7. Sun, G. *et al.* Layer-by-layer printing of laminated graphene-based interdigitated microelectrodes for flexible planar micro-supercapacitors. *Electrochem. commun.* **51**, 33–36 (2015).
8. Kurra, N., Ahmed, B., Gogotsi, Y. & Alshareef, H. N. MXene-on-Paper Coplanar Microsupercapacitors. *Adv. Energy Mater.* **6**, 1601372 (2016).
9. Peng, Y.-Y. *et al.* All-MXene (2D titanium carbide) solid-state microsupercapacitors for on-chip energy storage. *Energy Environ. Sci.* **9**, 2847–2854 (2016).
10. El-Kady, M. F. *et al.* Engineering three-dimensional hybrid supercapacitors and microsupercapacitors for high-performance integrated energy storage. *Proc. Natl. Acad. Sci.* **112**, 4233–4238 (2015).
11. Zhang, C. *et al.* Additive-free MXene inks and direct printing of micro-supercapacitors.

Nat. Commun. **10**, 1795 (2019).

12. Wu, Z.-S. *et al.* Alternating Stacked Graphene-Conducting Polymer Compact Films with Ultrahigh Areal and Volumetric Capacitances for High-Energy Micro-Supercapacitors. *Adv. Mater.* **27**, 4054–4061 (2015).

13. Yoo, J. J. *et al.* Ultrathin planar graphene supercapacitors. *Nano Lett.* **11**, 1423–1427 (2011).

14. Sollami Delekta, S., Smith, A. D., Li, J. & Östling, M. Inkjet printed highly transparent and flexible graphene micro-supercapacitors. *Nanoscale* **9**, 6998–7005 (2017).

15. Liu, W.-W., Feng, Y.-Q., Yan, X.-B., Chen, J.-T. & Xue, Q.-J. Superior Micro-Supercapacitors Based on Graphene Quantum Dots. *Adv. Funct. Mater.* **23**, 4111–4122 (2013).